Durham Research Online

Holographic generation of microtrap arrays
for single atoms by use
of a programmable phase modulator

**Silvia Bergamini, Benoît Darquié, Matthew Jones, Lionel Jacubowiez, Antoine Browaeys,
and Philippe Grangier**

Laboratoire Charles Fabry de l'Institut d'Optique, Centre Universitaire, Bâtiment 503, F-91403 Orsay, France

We have generated multiple micrometer-sized optical dipole traps for neutral atoms using holographic techniques with a programmable liquid-crystal spatial light modulator. The setup allows storing of a single atom per trap and addressing and manipulation of individual trapping sites. © 2004 Optical Society of America

OCIS codes: 020.7010, 140.7010, 090.1760, 090.2890.

1. INTRODUCTION

In the search for a suitable system for quantum information processing, certain requirements must be met,[1] such as scalability of the physical system, the capability of initializing and reading out the qubits, and the possibility of having a set of universal logic gates. Neutral atoms are one of the most promising candidates for storing and processing quantum information. A qubit can be encoded in the internal or motional state of an atom, and several qubits can be entangled using atom–light interactions or atom–atom interactions. Schemes for quantum gates for neutral atoms have been theoretically proposed that rely on dipole–dipole interactions[2–5] or controlled collisions.[6–9] Such schemes can be implemented in optical lattices with a controlled filling factor, as shown in Ref. 10, where multiparticle entanglement by means of controlled collisions was demonstrated.

Currently a major challenge is to combine controlled collisions with the loading and addressing of individually trapped atoms. Techniques to confine single atoms in micrometer-sized[11–13] or larger[14] dipole traps have been experimentally demonstrated. A set of qubits can be obtained by creating an array of such dipole traps, each storing a single atom.[15] Gate operations require the addressability of individual trapping sites and reconfigurability of the array. An array of dipole traps can be obtained by focusing a laser beam into a magneto-optic trap (MOT) with an array of microlenses, as demonstrated in Ref. 16, where each trap could be addressed individually but where each trapping spot still contained many atoms.

An alternative method to generate an array of small dipole traps is the use of holographic techniques. Holographic optical tweezers use a computer-designed diffractive optical element to split a single collimated beam into several beams, which are then focused by a high numerical aperture lens into an array of tweezers. Recently holographic optical tweezers were implemented by use of computer-driven liquid-crystal spatial light modulators (SLMs).[17] The advantage of these systems is that the holograms that correspond to various arrays of traps can be designed, calculated, and optimized on a computer. Then the traps can be controlled and reconfigured by writing these holograms on a SLM in real time. For example, each site can be moved and switched on and off independently from the others.

Here we present an experimental demonstration of the generation of multitrap arrays for single atoms. We use a SLM to control the optical potential of each trap and the geometry of the array, and our system allows each single-atom site to be addressed. This should open an avenue for qubit initialization and readout.

2. SPATIAL LIGHT MODULATOR

We used a Hamamatsu programmable phase modulator, PPM X7550, which includes a parallel-aligned (PAL) nematic liquid-crystal SLM. The SLM behaves as a mirror that can be used to encode a two-dimensional phase pattern on the reflected beam, thus acting as a phase grating that diffracts light. A prescribed amount of phase shift can be imposed by varying the local optical path length, which can be accomplished by controlling the local orientation of molecules in a layer of PAL nematic liquid crystals.

The structure of the device is described in Fig. 1. The PAL SLM module consists of a liquid-crystal layer deposited on a dielectric mirror. Behind the mirror there is an amorphous silicon photoconductive layer. This structure is sandwiched between two transparent electrodes. The orientation of the liquid-crystal molecules is determined by the electric field, which is controlled locally by changing the impedance of the photoconductive layer by use of a write beam, as shown in Fig. 1. The write beam is intensity modulated with a 480×480 pixel liquid-crystal device (LCD). We controlled each pixel individually by using a video graphics array (VGA) signal from a computer. The total active area of the SLM is $20\,\text{mm} \times 20\,\text{mm}$. We note that since the readout light is completely separated from the LCD, diffraction effects that are due to the pixellized structure almost vanish, and the optical quality can be very high.
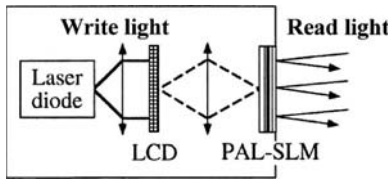
Fig. 1. Scheme of the SLM module X7550. The surface of the PAL SLM is 20 mm × 20 mm. The LCD is composed of 480 × 480 pixels and is controlled by a VGA signal.

We measured the optical properties of the PAL SLM by using a Zygo phase-shift interferometer operating at 633 nm. When the SLM is switched off, the reflectivity is greater than 90%, and the wave-front distortion is 0.6λ peak to peak over the whole surface and better than 0.1λ over an active area of side of 5 mm. We determined that the phase can be modulated between 0 and $2.1\,\pi$. For a given optical path length the phase shift is inversely proportional to the wavelength, so at our operating wavelength of 810 nm the maximum phase shift is reduced to $1.65\,\pi$.

3. HOLOGRAM GENERATION

We calculated the holograms by using an iterative fast Fourier transform algorithm, which exploits a numerical method to calculate the optimal phase modulation of the incident laser beam to obtain the desired intensity profile at the imaging plane.[18,19] This algorithm works in the case of phase-only holograms. We consider only regular arrays of optical traps, but the algorithm could be extended to more complicated structures with no lattice symmetries.

The basic idea is to find the relation between the intensity profile at the focal plane of the focusing objective that we want to obtain and the necessary phase modulation at the input plane. The wave front at the focal plane can be written as

$$E^f(\boldsymbol{\rho}) = E_0^f(\boldsymbol{\rho})\exp[i\,\phi^f(\boldsymbol{\rho})], \qquad (1)$$
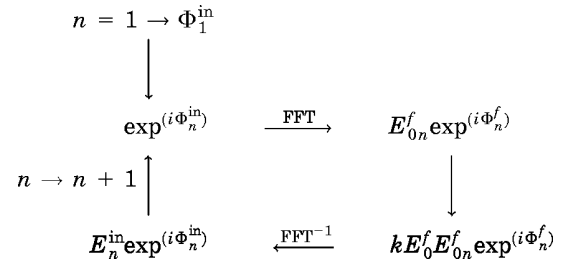
and $I^f(\boldsymbol{\rho}) = |E^f(\boldsymbol{\rho})|^2$ is the intensity profile that we want to obtain. The wave front at the entrance pupil of the focusing objective is

$$E^{\mathrm{in}}(\mathbf{r}) = E_0^{\mathrm{in}}(\mathbf{r})\exp[i\,\phi^{\mathrm{in}}(\mathbf{r})], \qquad (2)$$

where ϕ^{in} is the phase profile imposed by the hologram, which is the pattern we want to calculate. The input wave front can be written as the inverse Fourier transform of the wave front at the focusing plane:

$$E_0^{\mathrm{in}}(\mathbf{r})\exp[i\,\phi^{\mathrm{in}}(\mathbf{r})] = \mathcal{F}^{-1}\{E^f(\boldsymbol{\rho})\}. \qquad (3)$$

We start by designing the array of traps we want to obtain in the focal plane as an array of Dirac delta functions, and we obtain $E_0^f(\boldsymbol{\rho})$ by convoluting the array with an Airy pattern linked to the entrance pupil of the optical system. The algorithm is initialized by a guess of the phase distribution, which is used to calculate a pattern for the phase modulation of the input wave Φ_1^{in}, as shown in the following diagram. Amplitude E_0^{in} is chosen equal to one, as we do not change the amplitude of the input beam by modulating the phase only.

$$n = 1 \rightarrow \Phi_1^{\mathrm{in}}$$
$$\downarrow$$
$$\exp^{(i\Phi_n^{\mathrm{in}})} \xrightarrow{\mathrm{FFT}} E_{0n}^f \exp^{(i\Phi_n^f)}$$
$$n \rightarrow n+1 \uparrow \qquad\qquad \downarrow$$
$$E_n^{\mathrm{in}}\exp^{(i\Phi_n^{\mathrm{in}})} \xleftarrow{\mathrm{FFT}^{-1}} k E_0^f E_{0n}^f \exp^{(i\Phi_n^f)}$$

Following the above diagram, we can calculate the image on the focusing plane corresponding to this phase modulation at the input plane by Fourier transformation. The result will of course differ from the desired pattern. At this point we reduced the difference by multiplying the solution found by the desired pattern, $E_0^f(\boldsymbol{\rho})$. After normalizing this product (k being a constant to normalize the field amplitude), we took the inverse Fourier transform of the latter and we extracted a phase pattern for the input beam that is closer to the one required. Then the cycle was repeated. This kind of algorithm converges within three to four iterations.[18,19]

As examples of calculated holograms, Fig. 2 (left) shows the phase profile of the input wave used to obtain an array of three dipole traps in a row separated by 5 μm at the focusing plane of the objective. Figure 2 (right) shows the hologram calculated for obtaining an array of five dipole traps. These holograms were used to generate the trap arrays that will be presented in the following sections; see Fig. 6. These patterns are transmitted to the SLM by a standard VGA card. The different gray levels correspond to different phase shifts, with black and white giving a phase shift of $-\pi$ to π. We calculated the phase modulation, taking into account the size of the beam that illuminates the PAL SLM, so the modulated area in Fig. 2 corresponds to the size of the beam at the SLM position. Therefore only a fraction of the total area of the PAL SLM is active for phase modulation.

Once the hologram is calculated, it can be modified by changing several parameters: the modulation area of the SLM can be reduced, increased, or translated to optimize a match with the beam's size and position, and the modulation amplitude can be varied for optimal diffraction efficiency.

4. DIPOLE TRAP EXPERIMENT

Our apparatus, described in Refs. 11–13, consists of a strongly focused dipole trap loaded from a MOT for ru-
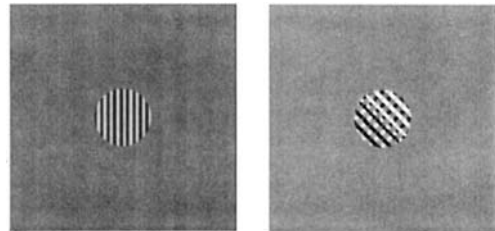

Fig. 2. Examples of two holograms calculated to generate an array of three dipole traps (left) and five traps in a cross configuration (right). The different gray levels correspond to different phase shifts, with black and white giving a phase shift of $-\pi$ to $+\pi$. For both holograms the separation between the traps in the focal plane of the objective is 5 μm and the pupil size is 5 mm.
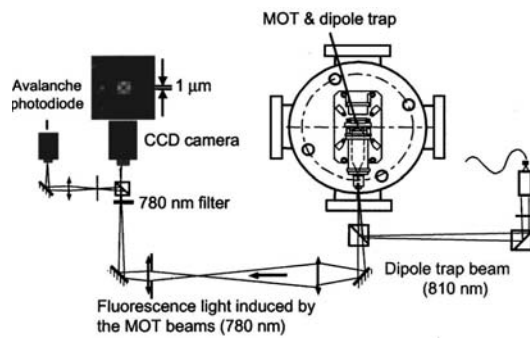
Fig. 3.   Experimental setup (without the SLM device). The focusing objective (inside the vacuum chamber) generates the dipole trap at the MOT position. An imaging system collects the fluorescent light from the trapped atoms and sends it to a CCD camera.
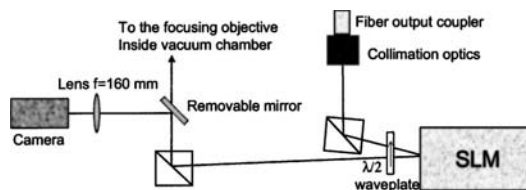

Fig. 4.   Experimental setup for phase modulation of the dipole trap beam. The removable mirror placed in the beam path is used to send light to an imaging camera that records the geometry and shape of the generated pattern.

bidium atoms. The MOT is loaded from an atomic beam, slowed down by chirped cooling. The dipole trap beam is focused by an objective placed inside the vacuum chamber (Fig. 3), with a numerical aperture of 0.7. This gives a measured beam waist of 0.9 μm, which is close to the diffraction limit.[12] The effective focal length is 3.55 mm. This focused beam provides a tightly confined trapping potential at the center of the intersection region of the MOT beams. With a relatively small laser power of 10 mW, very high intensities can be reached at the focusing position (1000 kW cm^{-2}). The dipole trap is operated in the far-detuned regime, the laser wavelength being 810 nm, to be compared with the rubidium atomic transitions D_1 at 795 nm and D_2 at 780 nm.

We detected the trapped atoms by using the fluorescence induced by the MOT beams at 780 nm. The fluorescence is collected by the same objective that focuses the dipole beam, and the detection system gives a magnified image of the trap on a charge-coupled device (CCD) camera, as shown in Fig. 3. A size of 1 μm on the focusing plane of the objective is imaged on 1 pixel of the CCD camera. The integration time is 200 ms.

The dipole trap can be operated in several loading regimes.[11,13] The loading rate of the dipole trap is proportional to the density of the MOT, which can be varied over several orders of magnitude by changing the intensity of the magnetic field gradient and the intensity of the slowing beams. When the MOT density is small (weak-loading regime) the lifetime of the atoms in the dipole trap is determined mainly by one-body decay that is due to collisions with the background gas. If the loading rate is increased, because of the small trapping volume, there is a range of loading rates for which two-body collisions

become the dominant term, allowing only one atom at a time to be stored in the trap. If a second atom enters the trap, a collision occurs and both atoms are ejected, as shown in Ref. 11. This collisional blockade mechanism operates only for very small trapping beam waists, typically less than 4 μm.[11] When the MOT density is high, the loading rate is so high that the average number of atoms in the trap can reach typically 30 (strong loading regime).

The dipole trap beam is produced by an 810-nm laser diode and brought to the experiment by use of an optical fiber, and the PAL SLM module is placed in the path of the dipole beam, as shown in Fig. 4. The beam waist at the SLM position was measured to be 2.3 mm, so that an area of $\simeq 15$ mm^2 of the SLM was illuminated. The power of the incident beam varied depending on the number of traps and trap depth that we wanted to obtain. The SLM can withstand laser intensities of up to 200 mW/cm^2. To maximize the diffraction efficiency the incident beam must be linearly polarized along the zero voltage direction of the molecules, which was ensured by placing a $\lambda/2$ plate in front of the SLM.

5. EXPERIMENTAL RESULTS

Here we show how arrays of traps with different geometries were created by sending holograms to the SLM. For simple geometries of the trap array, we can completely extinguish the trap corresponding to the zeroth-order diffraction spot. We also prove that we can control the position of the traps with micrometer precision. Finally, we used a simple array geometry to confine single atoms at distinct trapping sites.

A. Tests with Different Geometries
Different holograms were calculated with the iterative fast Fourier transform algorithm described in Section 3. Each calculated hologram was optimized with an auxiliary lens, with a focal length of 160 mm, focusing the generated pattern on a standard CCD camera (see Fig. 4).

As an example, the intensity profile of a three-spot array is shown in Fig. 5. The three-dimensional plot shows that the three spots have equal intensity. By adjusting the hologram, as explained in Section 3, we can optimize the symmetry of the intensity profile, remove higher-order diffraction spots, and control the zeroth order.

Fig. 5.   Two-dimensional and three-dimensional plots of the intensity profile generated by a three-spot hologram. The image was captured by focusing the diffracted beams onto a CCD camera by use of an auxiliary lens with 160-mm focal length.

The light was then sent to the atomic sample. We monitored the resulting fluorescence pattern and fine tuned the hologram to obtain the desired trapping configuration. The resulting fluorescence pattern from the trapped atoms for four different holograms is shown in Fig. 6. For these pictures we worked in the strong loading regime, and so each trap contains a few tens of atoms. Figure 6 (left) shows two traps generated symmetrically with respect to the zeroth order, which has been suppressed completely. The second and third panels of Fig. 6 show arrays of three dipole traps obtained by use of the phase modulation pattern shown in Fig. 2 (left), rotated by either 0° or 90° in the SLM plane. Finally five traps were generated by use of the hologram in Fig. 2 (right). The limited total laser power available did not allow us to test structures with a larger number of traps, but we have successfully calculated holograms with 3×3 symmetric spots and hexagonal geometries.

We limited our tests to two-dimensional geometries, but three-dimensional configurations are also possible. The focusing plane could be changed by adding a lens to the beam path so that its convergence can be changed. The effect of the lens can be easily reproduced by adding a quadratic phase modulation to the existing hologram. Therefore, by dynamically changing the computer signal sent to the SLM it is possible also to create a three-dimensional trap array and to change the geometry and the positions of the traps.[20,21]

B. Controlling the Zeroth Order

One of the main issues in using an essentially diffractive optical element is the zeroth-order diffraction spot. Although high diffraction efficiency can be achieved, the residual zeroth-order diffraction spot cannot always be easily controlled for the design of the pattern. Here we show that it is possible either to extinguish the trapping site associated with the zeroth-order beam completely or to exploit it to create arrays of equally intense traps.

Figure 7 shows the images taken for two and three traps. We note that the two traps are generated symmetrically with respect to the zeroth-order diffraction spot and that the middle trap in the three-trap array is generated with the zeroth order. We are therefore able to take into account the zeroth order in our calculations and to control finely its intensity, so that we can generate arrays of traps at which the zeroth order is suppressed. Actually, we exploit the experimental observation that there is a trapping depth threshold, below which the atoms cannot be captured. Therefore, the central peak actually disappears as soon as the intensity is below the threshold required to capture atoms, even if the trap light intensity has not completely vanished. This method provides good enough control that we are not limited by the zeroth-order diffraction spot for simple geometries.

C. Varying the Relative Distance

It is also possible to control fully the relative position of the trapping sites, either between experiments or dynamically, just by changing the hologram supplied to the device as a VGA signal. The lattice constant can therefore be changed as well as its geometry.

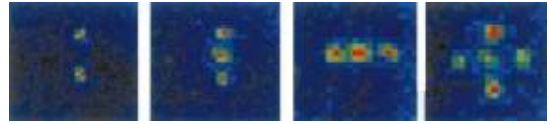This is illustrated in Fig. 8, where we show how to con-

Fig. 6.   MOT-induced fluorescence of trapped atoms in dipole trap arrays. The integration time of the CCD was set to 200 ms. The snapshots show the different geometries tested for a total laser power of 40 mW.
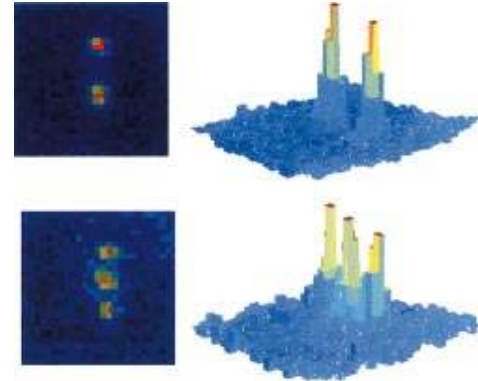

Fig. 7.   Fluorescent images for two-trap and three-trap arrays, showing control of the zeroth order. The two traps in the top figures were generated symmetrically with respect to the zeroth-order diffraction spot; the middle trap in the bottom figure was generated from the zeroth order.

Fig. 8.   MOT-induced fluorescence of trapped atoms in two dipole traps. The integration time of the CCD is 200 ms. The figures show how the distance could be varied with micrometer accuracy by sending a modified signal to the SLM.

trol the relative distance of two traps with micrometer accuracy. Trap separation δ in one array at the imaging plane depends on the periodicity of the phase modulation:

$$\delta = (\lambda f/p), \qquad (4)$$

where λ is the laser wavelength, f is the focal distance of the objective, and p is the phase modulation period. So in the case of simple geometries, where there is a lattice structure, the separation between the traps can be changed by modifying the period of the lattice. Our measurements were limited by the magnification of the imaging system for which 1 μm on the focusing plane is imaged on 1 pixel.

From Eq. (4) the minimum change in the trap separation is associated with the minimum change in the phase modulation period, which is given by the size of 1 pixel of the SLM ($\simeq 40$ μm). For our present (nonoptimized) setup and for the case of 4-μm separation in Fig. 8, this gives a precision limit of the trap position of 300 nm.

In more complicated geometries with many traps, the moving of only one of the traps with respect to the others can be achieved in real time by sending sequences of precalculated holograms to the SLM. Dynamic control of

the trap position is dependent on the response time of the SLM itself and on the update rate of the driving VGA signal. Currently the refresh rate of available systems with nematic crystals (including the Hamamatsu SLM used here) is limited to a few tens of hertz. Higher speed (in the kilohertz range) can be achieved, in principle, with commercial ferroelectric liquid crystals,[22] that have a lower diffraction efficiency. Therefore the current performance for the moving speed of the traps does not quite allow fast enough control for gate operations.

This limitation can be overcome by use of schemes that rely on the combination of an array of (slowly) reconfigurable traps and of a fast moving head, which can be realized with a laser beam driven by two-dimensional acousto-optic modulators (beam scanners). Such a scheme would be a neutral atom analog of the proposal for ion traps in Ref. 23.

D. Single Atom Trapping
Finally, we tested the hologram-generated three-trap configuration for single-atom trapping. By decreasing the density of the atomic cloud it is possible to enter the regime of loading in which either one or zero atom is trapped per each site. In Fig. 9 (left) a single atom is captured in one trap and its fluorescence is detected with a 200-ms integration time. On the right-hand side, two atoms are simultaneously loaded in two distinct traps. The traps are generated with a laser power of 4 mW for each one, which is just above the threshold laser power to capture one atom. Working close to the threshold trap intensity minimizes the light shift induced by the trapping beam and therefore maximizes the MOT-induced fluorescence signal for a single atom.

Some considerations can be made about the quality of the traps generated with the hologram. For example, by comparing the threshold laser power for traps generated by diffracted beams with the threshold laser power for trapping with a nondiffracted beam and assuming that the trapping threshold depends only on the depth of the trap, we can give a better estimate of the maximum beam-waist enlargement. The trap depth is proportional to the laser power and inversely proportional to the square of the beam waist, so if a change in laser power is necessary to reach the trapping threshold, this can easily be related to a change in beam size. From these considerations we estimate an upper limit for the waist enlargement of 15% with respect to a nondiffracted beam, which means an upper limit for the waist of the diffracted beams of just over 1 μm.

Fig. 9. MOT-induced fluorescence of single atoms confined in distinct dipole traps of a three-trap array, where the traps are separated by a few micrometers. The two figures show one atom captured in one of the traps and two atoms being simultaneously trapped in two traps of a three-trap array. The integration time of the CCD was set to 200 ms.

In the collisional blockade regime, two-body collisions lock the average number of atoms to 0.5.[11] This means that in these operating conditions the theoretical probability of detecting one atom in one of the traps is 0.5. The probability of detecting three atoms being simultaneously stored in three distinct traps therefore drops down to 0.125. Imbalance in the trap depth would further reduce this probability. Referring to Fig. 9 (right), we found that the trap that is not lit showed a probability of <0.5 of storing a single atom, which is probably due to a shallower trap depth, linked to an asymmetry in the generated intensity pattern.

6. CONCLUSION
We have demonstrated the possibility of creating multi-trap arrays for single atoms by using a nematic liquid-crystal spatial light modulator. The advantage of using such a device is that it is fully programmable and computer controllable: multiple traps can be generated in different geometries and the position of the traps can be designed from the VGA signal sent to the module. Arrays of traps, each capable of storing a single atom, can be dynamically modified, allowing real-time motion of one or more traps with respect to the array.

This opens up possibilities for testing the proposed schemes for atom–atom entanglement. For example, qubit encoding on the motional state of an atom in a dipole trap was proposed in Ref. 9. In another scheme[8] the qubit is encoded in the motional state of one atom, which can be trapped in either of two traps with an adjustable separation. Both proposals[8,9] were studied for rubidium microdipole traps for which single-atom storage was obtained with our setup. According to these proposals single-qubit operations could be achieved by moving the traps adiabatically and bringing them closer so that tunneling between the two wells is allowed, and two-qubit operations are achieved by collisions between two atoms stored in distinct traps.

Alternatively, qubits can be encoded in single atoms trapped at different locations by use of the hyperfine structure of the ground state, the initialization and single-qubit operations being achieved with Raman pulses. Two-qubit operations then require either controlled cold collisions as implemented recently[10] or long-range coupling as proposed in Refs. 2 and 3.

REFERENCES

1. D. P. DiVincenzo, "The physical implementation of quantum computation," Fortschr. Phys. **48**, 771–783 (2000).
2. I. E. Protsenko, G. Reymond, N. Schlosser, and P. Grangier, "Operation of a quantum phase gate using neutral atoms in microscopic dipole traps," Phys. Rev. A **65**, 052301 (2002).
3. D. Jaksch, J. I. Cirac, P. Zoller, S. L. Rolston, R. Côtè, and M. D. Lukin, "Fast quantum gates for neutral atoms," Phys. Rev. Lett. **85**, 2208–2011 (2000).
4. G. K. Brennen, I. H. Deutsch, and P. S. Jessen, "Entangling dipole–dipole interactions for quantum logic with neutral atoms," Phys. Rev. A **61**, 062309 (2000).
5. G. K. Brennen, C. M. Caves, P. S. Jessen, and I. H. Deutsch, "Quantum logic gates in optical lattices," Phys. Rev. Lett. **82**, 1060–1063 (1999).
6. T. Calarco, E. A. Hinds, D. Jaksch, J. Schmiedmayer, J. I. Cirac, and P. Zoller, "Quantum gates with neutral atoms: controlling collisional interactions in time-dependent traps," Phys. Rev. A **61**, 022304 (2000).
7. D. Jaksch, H.-J. Briegel, J. I. Cirac, C. W. Gardiner, and P. Zoller, "Entanglement of atoms via cold controlled collisions," Phys. Rev. Lett. **82**, 1975–1978 (1999).
8. J. Mompart, K. Eckert, W. Ertmer, G. Birkl, and M. Lewenstein, "Quantum computing with spatially delocalized qubits," Phys. Rev. Lett. **90**, 147901 (2003).
9. K. Eckert, J. Mompart, X. X. Yi, J. Schliemann, D. Bruss, G. Birkl, and M. Lewenstein, "Quantum computing in optical microtraps based on the motional states of neutral atoms," Phys. Rev. A **66**, 042317 (2002).
10. O. Mandel, M. Greiner, A. Widera, T. Rom, T. W. Hänsch, and I. Bloch, "Controlled collisions for multi-particle entanglement of optically trapped atoms," Nature (London) **425**, 937–940 (2003).
11. N. Schlosser, G. Reymond, and P. Grangier, "Collisional blockade in microscopic optical dipole traps," Phys. Rev. Lett. **89**, 23005 (2002).
12. G. Reymond, N. Schlosser, I. Protsenko, and P. Grangier, "Single-atom manipulations in a microscopic dipole trap," Philos. Trans. R. Soc. London, Ser. A **361**, 1527–1536 (2003).
13. N. Schlosser, G. Reymond, I. Protsenko, and P. Grangier, "Sub-poissonian loading of single atoms in a microscopic dipole trap," Nature (London) **411**, 1024–1026 (2001).
14. D. Frese, B. Ueberholz, S. Kuhr, W. Alt, D. Schrader, V. Gomer, and D. Meschede, "Single atoms in an optical dipole trap: towards a deterministic source of cold atoms," Phys. Rev. Lett. **85**, 3777–3780 (2000).
15. S. Kuhr, W. Alt, D. Schrader, I. Dotsenko, Y. Miroshnychenko, W. Rosenfeld, M. Khudaverdyan, V. Gomer, A. Rauschenbeutel, and D. Meschede, "Coherence properties and quantum state transportation in an optical conveyor belt," Phys. Rev. Lett. **91**, 213002 (2003).
16. R. Dumke, M. Volk, T. Müther, F. B. J. Buchkremer, G. Birkl, and W. Ertmer, "Micro-optical realization of arrays of selectively addressable dipole traps: a scalable configuration for quantum computation with atomic qubits," Phys. Rev. Lett. **89**, 097903 (2002).
17. D. G. Grier, "A revolution in optical manipulation," Nature (London) **424**, 810–816 (2003).
18. V. A. Soifer, V. V. Kotlyar, and L. L. Doskolovich, *Iterative Methods for Diffractive Optical Elements Computation* (Taylor & Francis, London, 1997).
19. E. R. Dufresne, G. C. Spalding, M. T. Dearing, S. A. Sheets, and D. G. Grier, "Computer-generated holographic optical tweezer arrays," Rev. Sci. Instrum. **72**, 1810–1816 (2001).
20. J. E. Curtis, B. A. Koss, and D. G. Grier, "Dynamic holographic optical tweezers," Opt. Commun. **207**, 169–175 (2002).
21. H. Melville, G. F. Milne, G. C. Spalding, W. Sibbett, K. Dholakia, and D. McGloin, "Optical trapping of three-dimensional structures using dynamic holograms," Opt. Express **11**, 3562–3567 (2003), http://www.opticsexpress.org.
22. W. J. Hossack, E. Theofanidou, J. Crain, K. Heggarty, and M. Birch, "High-speed holographic optical tweezers using a ferroelectric liquid crystal microdisplay," Opt. Express **11**, 2053–2059 (2003), http://www.opticsexpress.org.
23. J. I. Cirac and P. Zoller, "A scalable quantum computer with ions in an array of microtraps," Nature (London) **404**, 579–580 (2000).